Homogeneous $U_{0.89}Pu_{0.11}O_2$ mixed oxide by use of PuO_2 nanopowders

Boshoven, Jacobus; Ndiaye, Abibatou; Morel, Bertrand; Cologna, Marco; Vigier, Jean François; Carlos Marquez, Ramon; Konings, Rudy J.M.; Popa, Karin

DOI
10.1016/j.jnucmat.2025.155915

Publication date
2025

Document Version
Final published version

Published in
Journal of Nuclear Materials

Journal of Nuclear Materials 614 (2025) 155915

Contents lists available at ScienceDirect

Journal of Nuclear Materials

journal homepage: www.elsevier.com/locate/jnucmat

Homogeneous $U_{0.89}Pu_{0.11}O_2$ mixed oxide by use of PuO_2 nanopowders

Jacobus Boshoven [a], Abibatou Ndiaye [b], Bertrand Morel [c], Marco Cologna [a,*], Jean-François Vigier [a], Ramon Carlos Marquez [a], Rudy J.M. Konings [a,d], Karin Popa [a,*]

[a] European Commission, Joint Research Centre (JRC), Karlsruhe, Germany
[b] ORANO Projects, MELOX, Les Tourettes, D138A, 30200, Chusclan, France
[c] ORANO Support, 92320 Châtillon, France
[d] Faculty of Applied Sciences, Radiation Science & Technology Department, Delft University of Technology, Mekelweg 15, Delft 2629JB, the Netherlands

GRAPHICAL ABSTRACT

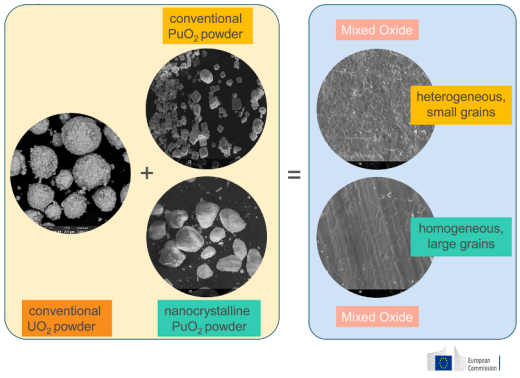

ARTICLE INFO

Keywords:
Mixed oxides
Nanocrystals
Nuclear fuel
Diffusion

ABSTRACT

We show that a homogeneous single-phase mixed oxide is obtained by blending and sintering commercial UO_2 and nanocrystalline PuO_2 powder; whereas, under the same conditions, conventional PuO_2 powder obtained from oxalate precipitation and composed of platelets, yields two-phase mixed oxide. The use of nanometric PuO_2 results in a larger final grain size.

1. Introduction

Metal oxide powder technology is widely used for the preparation of technical ceramics [1]. The quality of the final products strongly depends on a multitude of process parameters, from the starting materials via the forming techniques to the heat treatment. Nuclear oxide fuel is a typical product of such powder technology. Uranium oxide fuel for Light Water Reactors (LWR) has a straightforward cylindrical form. These pellets are made from a powder blend of "fresh" UO_2 powder obtained by conversion of UF_6 enriched in fissile ^{235}U, for example via the ADU (ammonium diuranate) or AUC (ammonium uranyl carbonate) routes, and scrap powder obtained from crushing and milling rejected pellets

* Correspinding authors.
E-mail addresses: marco.cologna@ec.europa.eu (M. Cologna), karin.popa@ec.europa.eu (K. Popa).

https://doi.org/10.1016/j.jnucmat.2025.155915
Received 28 March 2025; Received in revised form 19 May 2025; Accepted 20 May 2025
Available online 21 May 2025

and grinding dust. The powder is compacted in a press, then the green pellets obtained are sintered at high temperature and finally ground to the right diameter since sintering leads to an anisotropic shrinkage of the pellets. This process is implemented at industrial level in a continuous way. Mixed oxide (MOX) fuel for LWRs, in which reprocessed plutonium is used as fissile material, is made in a slightly different manner, which has its origin in the fact that direct mixing of the two powders results in a heterogenous product in which the Pu-rich phase has a Pu concentration that makes it insoluble in the PUREX fuel reprocessing process. At a concentration of $Pu/(U+Pu) < 0.3$ in the $(U,Pu)O_2$ solid solution, dissolution in nitric acid occurs with acceptable kinetics. For that reason the industrial LWR MOX fabrication is a two-step process. First a master blend is produced from natural or depleted uranium oxide and the plutonium oxide (around 30 % PuO_2) which is next blended down to the required plutonium concentration with UO_2 powder [2]. The product of this so-called MIMAS process (MIcronized - MASter blend) is macro-homogeneous/micro-heterogeneous, with Pu-rich areas in a U-rich matrix, which leads to differences in the in-pile behaviour between UO_2 and MOX fuel.

An alignment of the in-pile behaviour of the two fuel types can be obtained by a better homogenisation of plutonium in the MOX fuel, which can be realised by changes in the used powder technology. Of the numerous options (*e.g.* optimized co-milling, short binder-less route, co-precipitation/decomposition, freeze-granulation etc.), we report here on a study of a change of the PuO_2 powder characteristics. In the current industrial process, the PuO_2 is obtained by oxalate precipitation of the reprocessed plutonium. This yields a powder of platelet-like aggregates, which is not ideal for powder blending [3]. The recent advances in producing nanocrystalline (***nc***) actinide oxide particles have revealed that hydrothermal decomposition yields aggregates of spherical morphology, similar to the ADU UO_2 powder [4]. It is thus interesting to compare the two plutonium oxide powders in a powder blending process to explore the effect on the fuel microstructure. In this article, we report results of small-scale laboratory experiments to assess the possible improvements the use of ***nc***-PuO_2 can bring in the mixed oxide fuel production.

2. Materials and methods

2.1. Characterisation techniques

2.1.1. Density measurements

For powder density measurements, the powders were gently filled in a 10 mL glass cylinder. The weights of filled powder were measured and the volume was read from the filled cylinder. These data were used to calculate the bulk density. The cylinder was then gently shaken and tapped until the powder volume showed no further decrease. These volumes together with the weight were used to calculate the tap density.

The geometrical densities of all pellets were calculated from the measured weight (Mettler-Toledo AG204), diameter and height (Mitutoyo QuickMike). Heights were measured several times and the diameter was measured at several heights and angles and the averaged values were used in the calculations. The hydrostatic (Archimedes) density was measured using a Sartorius BP211D balance equipped with a density unit.

2.1.2. Powder X-ray diffraction

The crystalline structure/purity of the products was determined at room temperature by powder XRD using a Bruker D8 X-ray diffractometer mounted in a Bragg–Brentano configuration with a curved Ge monochromator (1,1,1) and a copper tube (40 kV, 40 mA) equipped with a LinxEye position sensitive detector. For the measurement, the ground powders were immobilised in a bi-component epoxy resin on a sample holder. Structural analyses were performed with the JANA 2006 software suite [5] using the Loopstra-Rietveld method [6]. When possible, values of the crystallite sizes were calculated using the Williamson-Hall plot [7].

2.1.3. Scanning electron microscopy

Images of the PuO_2 powders and the $(U,Pu)O_2$ pellets were obtained using a Philips/FEI™ XL40 SEM operated at 25 kV, equipped with a SAMx Energy Dispersive X-ray analysis system (EDX) based on a Liquid Nitrogen-free Silicon Drift Detector. This microscope (high-voltage unit, column, chamber, and turbomolecular pump) was placed inside a glovebox, while the components that are not getting in contact with the active materials (primary vacuum system, the water-cooling circuit, and the acquisition electronic) were outside.

2.2. Uranium dioxide and conventional plutonium dioxide

Uranium dioxide powder of depleted uranium from COGEMA TU2 stock (prepared by ammonium diuranate wet route) was used for the fabrication of the mixed oxide pellets without further treatment. XRD analysis (Fig. 1***a***) showed that the starting material consisted of a mixture of two phases: about 66 % of a phase with a lattice parameter of 5.464 Å that corresponds to a stoichiometry of $UO_{2.06}$, and 34 % of a second phase with a lattice of 5.442 Å, corresponding to U_4O_9 (or similar); this resulted in a total stoichiometry of about $UO_{2.12}$. SEM image (Fig. 1***b***) indicated that the powder consisted of soft spherical agglomerates.

The conventional PuO_2 from JRC stock was produced by thermal decomposition of oxalate. It was a pure single phase corresponding to $PuO_{2.00}$ with a lattice parameter of 5.4115 Å (Fig. 2***a***). This is 0.27 % larger than fresh PuO_2 (5.397 Å), in very good agreement with $PuO_{2.00}$ saturated with alpha damage [8]. The crystallites size was 175±75 nm, which due to the large uncertainty must be considered only as indicative. SEM images indicated formation of mostly platelet-like aggregates of PuO_2 (Fig. 2***b***). This crystalline powder is referred further as ***c***-PuO_2 (conventional).

2.3. Conversion to nanocrystalline PuO_2

The nanocrystalline PuO_2 powder (referred further as ***nc***-PuO_2) was produced by hydrothermal decomposition of oxalate originally described in [4]: 2.585 g PuO_2 powder was quantitatively dissolved in 33 mL aqueous solution of 14 mol/L HNO_3 and 0.04 mol/L HF. The dissolution process was performed at 160 °C for 28 h in a round-bottom flask made of Teflon. A volume of 27 mL of a clear Pu^{4+} aqueous solution was obtained. No spectroscopic characterisation was performed, but the colour of the solution corresponded to the tetravalent oxidation state of plutonium in aqueous solution. The plutonium solution was precipitated at ambient temperature (without further dilution) by pipetting it dropwise in an aqueous solution of 0.5 mol/L oxalic acid (20 % excess). The readily formed precipitate was separated from the acidic solution and washed repeatedly with small volumes of milli-Q® water until pH = 7. After filtration and drying, 4.037 g of hydrated plutonium oxalate was isolated. The hydrothermal decomposition process was performed in autoclaves made of stainless steel containing Teflon insets (with an available volume of about 12 mL). The Pu-oxalate was split in two equal portions of 1.91 g and placed in the Teflon insets of two identical autoclaves together with 5 mL of milli-Q® water and a magnetic stirrer. The hydrothermal treatment ran for 24 h at 220 °C at autogenic pressure with stirring (100 rpm). After cooling, the decomposition products were collected in a 50 mL Eppendorf® tube, then washed with milli-Q® water, ethanol and acetone. A small amount was collected for powder XRD characterization. The total amount of nanometric sized PuO_2 powder was 2.142 g (including the amount used for the XRD characterisation and associated losses during preparation). Thus, the conversion of bulk to ***nc***-PuO_2 was achieved with a yield of about 83 % over all these process steps.

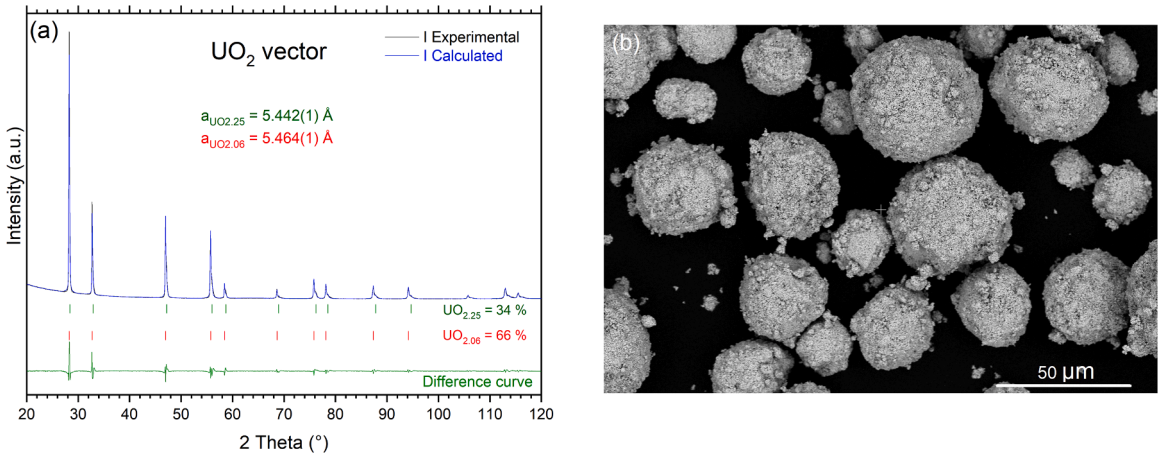

Fig. 1. (a) XRD pattern and Loopstra-Rietveld refinement of the UO_2 source material. (b) SEM image of the UO_2 powder used in the present study.

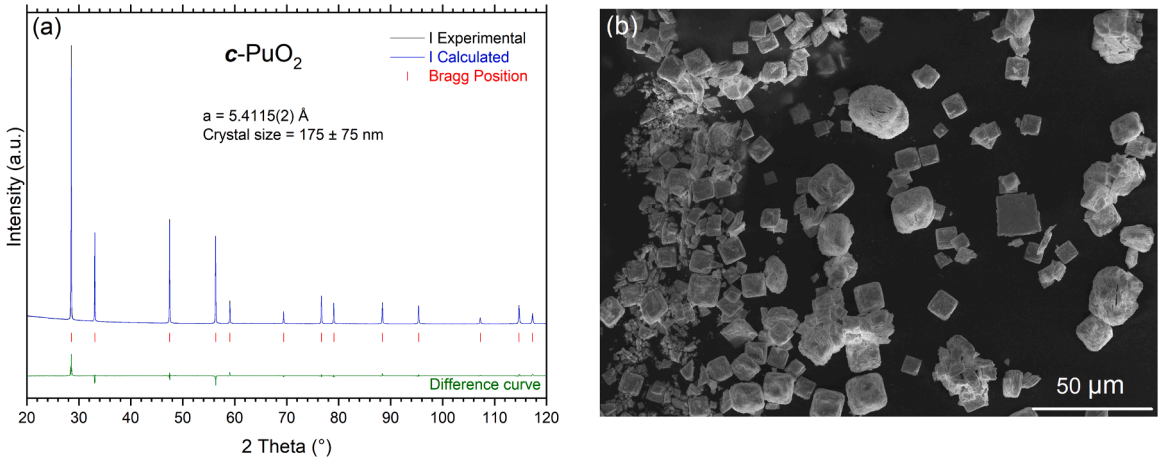

Fig. 2. (a) XRD pattern and Loopstra-Rietveld refinement of the ***c***-PuO_2 source material. (b) SEM image of the ***c***-PuO_2 material used in the present study.

2.4. Production of mixed oxide pellets

The UO_2 and PuO_2 oxide powders were mixed by weight, targeting a plutonium content of Pu/(*U*+Pu) = 0.11 (Table 1). The powder mixture was dry-milled in a vibratory mill (Retsch MM301) using a 25 mL ZrO_2 container. The milling process was conducted in two phases: the first for 159 min at a speed of 15 s^{-1}, and the second for 297 min at a speed of 20 s^{-1}, with four cooling breaks in between. During this process, three zirconia balls, each with a diameter of 12 mm and a mass of 5.4 g, were included in the container. Contrary to the industrial MIMAS process, the experiments were performed without scrap powder. Table 1 summarises the powder densities obtained after milling.

Each powder mixture was compacted in ten pellets and two discs using a Lauffer VIUG16 bi-directional press (die diameter 7.2 mm at a pressure of 380 MPa). The dimensions and the green densities of the fabricated pellets/discs are summarised in Table 2; a theoretical density of 11.01 g/cm^3 was derived from the endmembers for the specified composition and utilised for calculations. The powder mixture did not contain any additives and/or lubricant but the internal surface of the die was lubricated by pressing pellets from pure zinc stearate.

Of each batch, five pellets and one discs were selected and sintered under reductive gas in a cold wall Degussa VSL10/18 sintering furnace (parameters summarised in Table 3). The pellets/discs were placed in a

Table 1
Masses of the oxide powders and the bulk/tap densities.

	m UO_2, g	m PuO_2, g	bulk density, g/cm^3	tap density, g/cm^3
Mixed oxide from ***c***-PuO_2	15.4632	1.9149	2.75	2.98
Mixed oxide from ***nc***-PuO_2	15.4854	1.9164	4.03	4.21

Table 2
Geometrical dimensions and green densities of the mixed oxide pellets/disks.

	from ***c***-PuO_2	from ***nc***-PuO_2
Average height of pellets, mm	5.49(5)	5.41(5)
Average diameter of pellets, mm	7.27(5)	7.27(5)
Average height of discs, mm	1.34(1)	1.71(1)
Average diameter of discs, mm	7.28(1)	7.27(1)
Green density, % TD	65.2 ± 0.2	66.1 ± 0.4

Table 3
Parameters used during the sintering of the compacted pellets/disks.

Ramp, °C/h	Dwell, h	Temperature, °C	Gas
200		600	Ar/H_2
	2	600	Ar/H_2 + 1200 ppm H_2O
200		1700	Ar/H_2 + 1200 ppm H_2O
	4	1700	Ar/H_2 + 1200 ppm H_2O
200		600	Ar/H_2 + 1200 ppm H_2O
	1	600	Ar/H_2
200		25	Ar/H_2

molybdenum crucible. The temperature of the furnace was measured with a thermocouple type C, placed close to the samples. The Ar + 6 % H_2 sintering gas was moisturized with 1200 ppm of water vapour.

3. Results

3.1. Characterisation of nc-PuO_2

The XRD analysis indicated the presence of a pure nanocrystalline phase of PuO_2 (Fig. 3***a***). The Loopstra-Rietveld refinement resulted in a lattice parameter of 5.398(1) Å, in good agreement with values reported for nanocrystalline PuO_2 powders produced with the same technique earlier [4,9–11]. The broad diffraction peaks obtained for this material were characteristic of a nanocrystalline material, and gave a crystallite size value of 18 ± 3 nm.

SEM images taken of the ***nc***-PuO_2 (Fig. 3***b***) indicated that the powder consisted of soft spheroid agglomerates, in contrast to the platelet-like morphology specific to the aggregates resulting from thermal decomposition (for comparison, see Fig. 2***b***).

3.2. Characterisation of mixed oxide pellets

3.2.1. Pellet density

The results of the density measurements are presented in Table 4. Both geometrical and hydrostatic densities of the sintered pellets were superior to 97 % TD, with a very narrow variation between individual specimens. The density of the mixed oxide from ***nc***-PuO_2 remained slightly higher, in accordance with the higher green density. It is interesting that the small density difference observed for the green pellets is maintained after sintering, indicating that the extent of densification during sintering is the almost same for the two types of compacts.

3.2.2. XRD analysis

Fig. 4***a*** shows the XRD patterns of the mixed oxide sintered compacts obtained by conventional PuO_2 powders. Closer look at the high-angle region showed an obvious peak separation in the 112 – 118 2θ region (Fig. 4***b***), partially overlapping on the diffractogram and creating a shoulder in the diffraction peaks. It indicates a mixture of two cubic *fcc* phases of (U,Pu)O_2, one U-rich and one Pu-rich (Fig. 5). The two phases have a lattice parameter of 5.4694(5) Å (25 % of the mixture) and 5.4616(5) Å (75 % of the mixture), respectively, which results in a weighted average lattice parameter a of 5.4636 Å. The corresponding phases are $(U_{0.975}Pu_{0.025})O_2$ and $(U_{0.87}Pu_{0.13})O_2$, respectively, according to Vegard's law. By combining the phase proportion obtained from Rietveld refinement, and their composition deduced from their lattice parameters through the Vegard's law, we obtain an overall Pu/(U+Pu) ratio of 0.105, in excellent agreement with the targeted value.

Table 4
Average densities (% TD) of pellets before (geometrical measurements) and after sintering (geometrical and hydrostatic measurements).

	Before sintering	After sintering	
	Geometrical	Geometrical	Hydrostatic
MOX from ***c***-PuO_2	65.2 ± 0.2	97.3 ± 0.2	98.2 ± 0.2
MOX from ***nc***-PuO_2	66.1 ± 0.4	98.0 ± 0.2	98.5 ± 0.2

The XRD analysis performed on the mixed oxide sintered compacts prepared with ***nc***-PuO_2 (Fig. 4***c***) indicated the presence of a single, well crystalline cubic phase with symmetrical peaks in the same 112 – 118 2θ region (Fig. 4***d***). The lattice parameter of a = 5.4635(5) Å corresponded to the desired $U_{0.89}Pu_{0.11}O_2$ composition (within the error bar of the measurement).

3.2.3. Microstructural characterisation

SEM images of the free and fracture surfaces of the sintered mixed oxides pellets are shown in Fig. 6, while the elemental mapping of the actinides from EDX is presented in Fig. 7. In both cases the fracture was mostly transgranular (Fig. 6***c*** and ***d***), indicating that the grain boundary strength was higher than the bulk strength [14]. The grain size of the ***nc***-PuO_2 sample was clearly larger than the ***c***-PuO_2 (the surface grain size is 2 μm and 9 μm, respectively, as estimated from Fig. 6***a*** and ***b*** with the line intercept method without correction factor).

Moreover, the material produced from ***nc***-PuO_2 showed a significant fraction of symmetric triple grain boundary junctions with near 120 degrees angles, typical for materials in which grain growth has progresses well towards a microstructure with smooth grain boundaries that are no longer very mobile [15]. In contrast, the microstructure of the material produced from ***c***-PuO_2 showed a wide range of junctions typical for materials with rough grain boundaries that are still mobile. The porosity observed in the microstructure looks completely closed (Fig. 6), as expected from the high relative density measured (> 0.97 TD).

The two-phase nature of the ***c***-PuO_2 pellets evidenced by XRD is not caught by the elemental distribution maps of U and Pu (Fig. 7). Both samples look fairly homogeneous, possibly because the composition of the two phases is similar – $(U_{0.975}Pu_{0.025})O_2$ and $(U_{0.87}Pu_{0.13})O_2$ – or because the dis-homogeneity is of the same order of magnitude as the

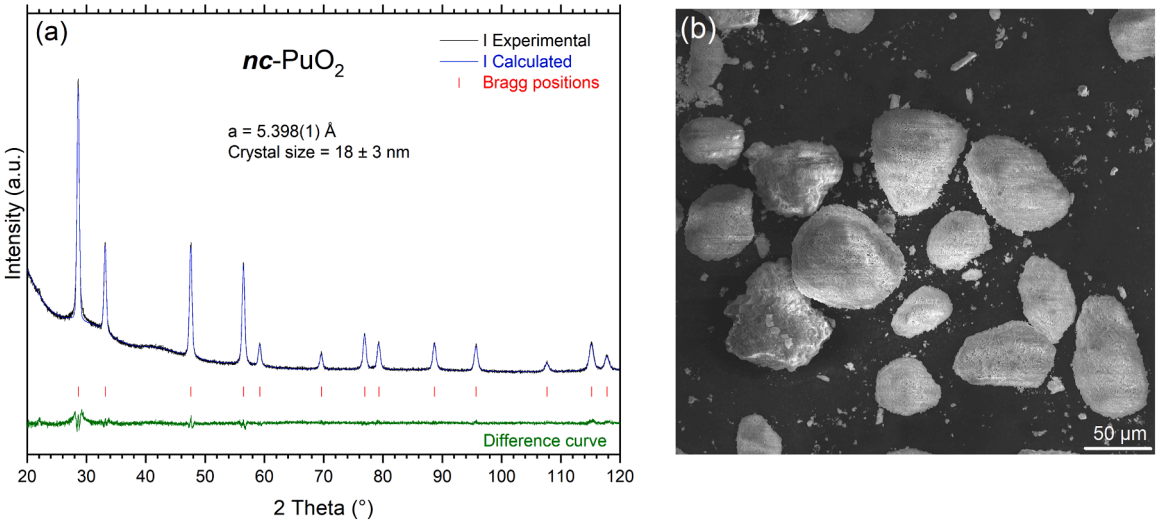

Fig. 3. (a) XRD pattern and Rietveld refinement of the ***nc***-PuO_2 material. (b) SEM image of the ***nc***-PuO_2 material.

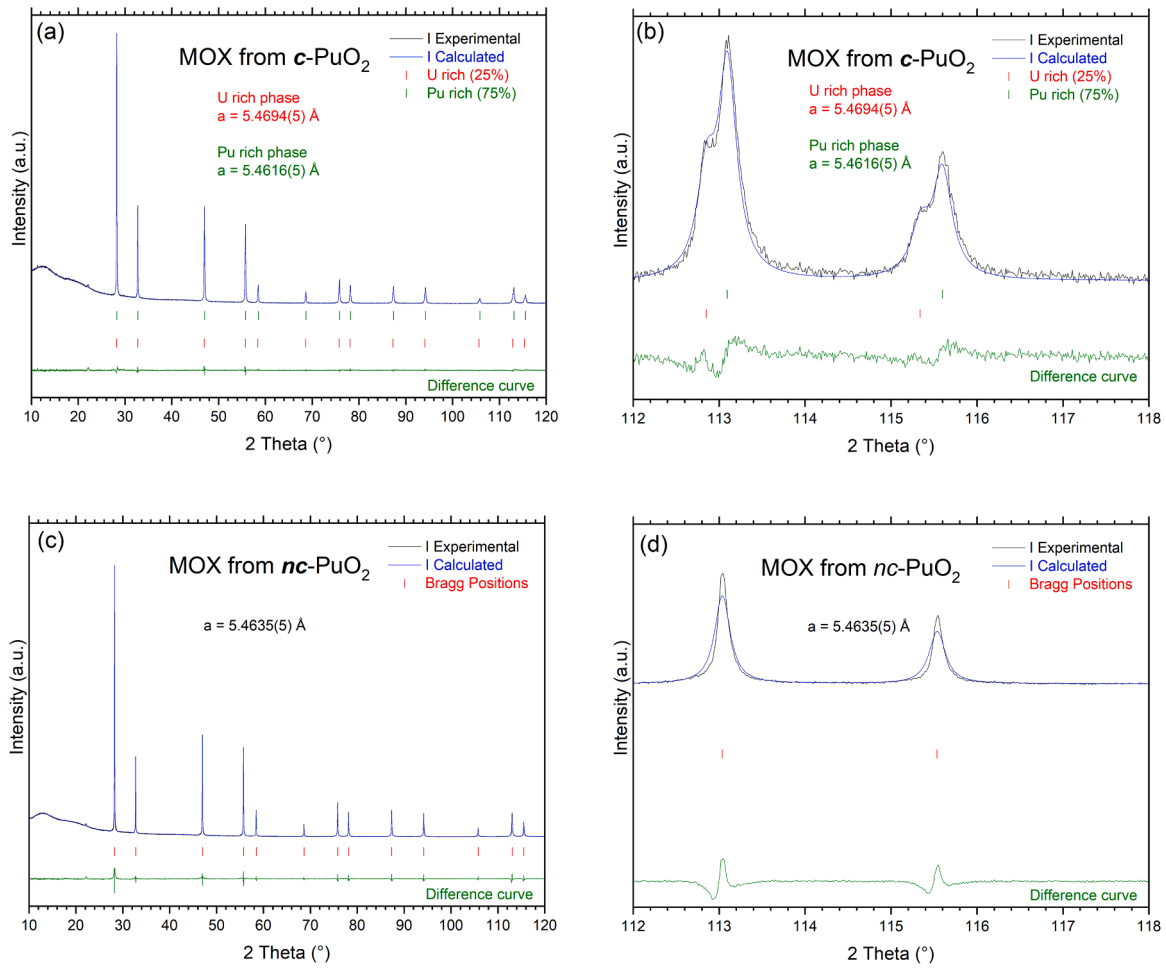

Fig. 4. XRD patterns and Loopstra-Rietveld refinement of mixed oxide materials obtained from ***c***-PuO_2 (a) and ***nc***-PuO_2 (c) powders. Detailed high-angle region, indicating the formation of a biphasic system in the case of the mixed oxide formed out of ***c***-PuO_2 (b) and a single phase formed out of ***nc***-PuO_2 (d).

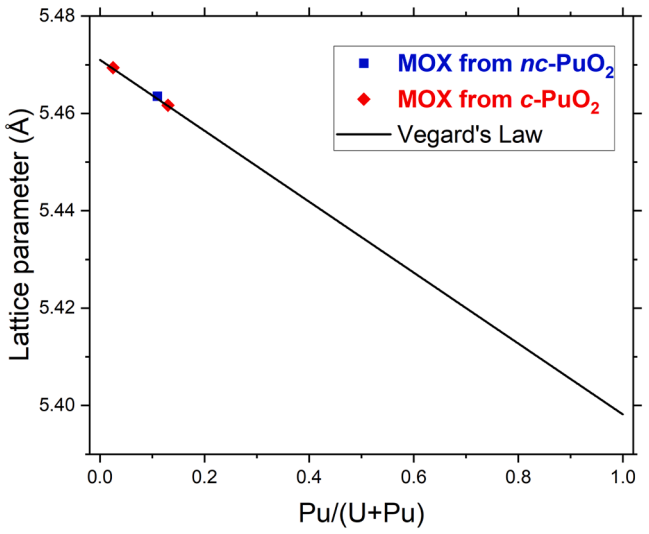

Fig. 5. Lattice parameters variation of the mixed oxide phases formed during the current experiments, following a Vegard's law drawn between the end members $UO_{2.00}$ (a = 5.47127 Å [12]) and PuO_2 (a = 5.39819 Å [13]).

spot size (~1 μm). In any case, large PuO_2 agglomerates/hot-spots [16] were not observed by EDX. More in-detail analysis were not performed.

4. Discussion

The current study has revealed a remarkable effect of the use of ***nc***-PuO_2 powder on the microstructure of mixed oxide fuel pellets prepared by powder technology. The better distribution of Pu in the product and the substantial larger grain size are clear indications that the use of ***nc***-PuO_2 powder results in a significantly higher driving force for uranium and plutonium interdiffusion during sintering compared to the material produced from standard PuO_2. This results in a dense, homogeneous microstructure with significantly larger grain size compared to the counterpart made from PuO_2 powder obtained in a conventional way. Other methods proposed for producing homogeneous MOX fuel include the freeze granulation route [17], but with no evidence of increasing the grain size. The decomposition of mixed oxalates at mild temperatures [18] also results in a homogeneous distribution of the actinides in the mixed oxide powders; however, no studies are available on their sintering behaviour. A large grain size is obtained in UO_2 fuel with the addition of chromium (Cr-doped fuel), which is one of the accident-tolerant fuel (ATF) concepts that have emerged in the recent years. Grain growth can also be achieved in MOX fuel by adding chromium. One of the anticipated advantages of large grain fuel is a better fission gas retention due to the larger grain size [19], resulting from the longer diffusion path to the grain boundaries, and thus delay the start of the faster grain boundary diffusion. It has been shown previously that

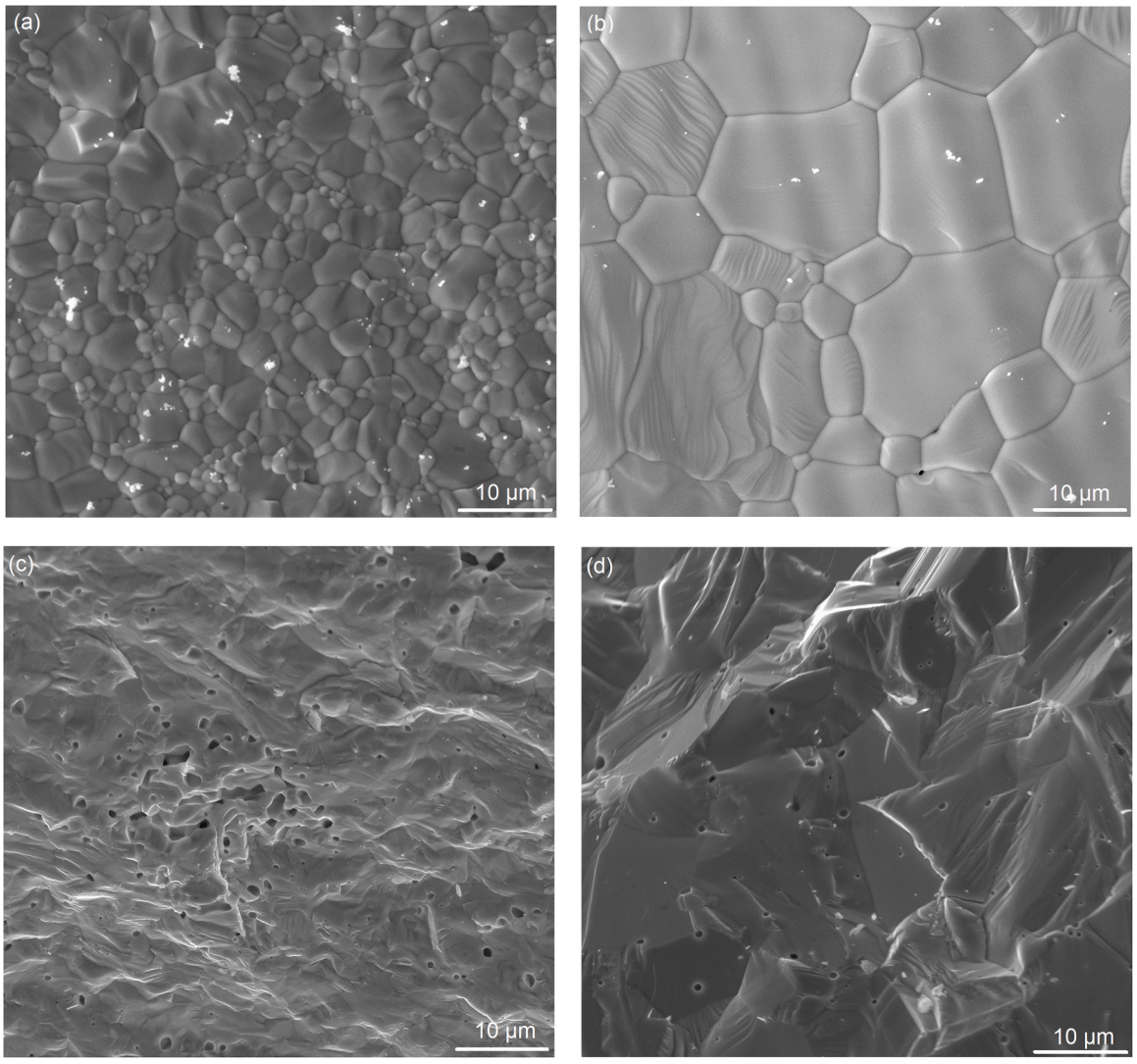

Fig. 6. SEM images of the free surfaces of the sintered mixed oxides pellets produced from ***c***-PuO_2 (a) and from ***nc***-PuO_2 (b). SEM images of the broken surfaces of the sintered mixed oxides pellets produced from ***c***-PuO_2 (c) and from ***nc***-PuO_2 (d).

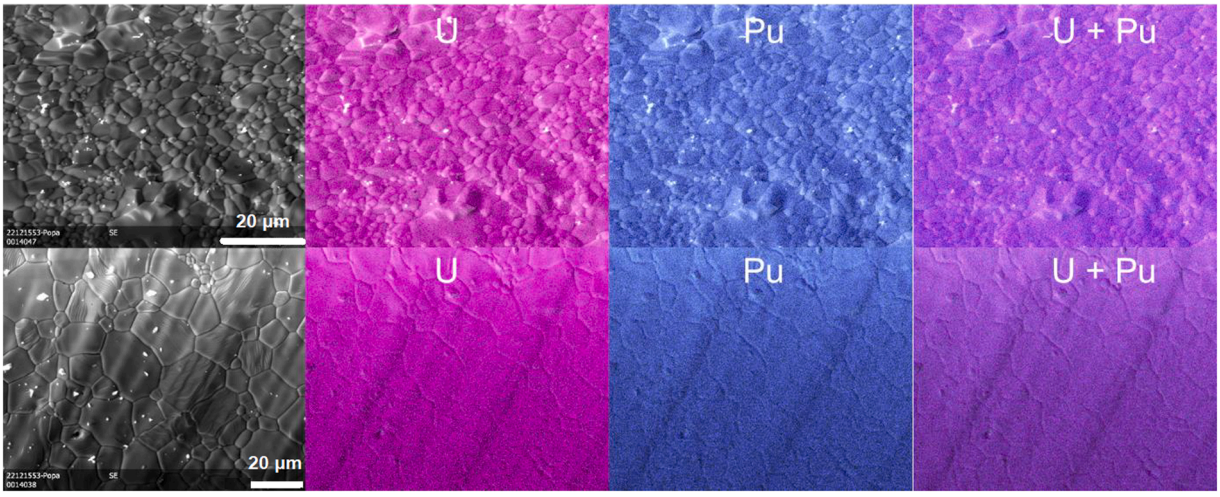

Fig. 7. EDX-mapping of Uranium and Plutonium in pellets of mixed oxides produced from ***c***-PuO_2 (top row) and ***nc***-PuO_2 (bottom row).

increasing the homogeneity of the initial MOX powder via liquid routes such as sol-gel, gives a larger final grain size, even in the absence of sintering additives such as chromium [20]. Here we show that this is also achievable by only modifying the properties of the powder which constitutes the smaller fraction (11 % nano-PuO_2), while keeping the UO_2 powder and all other processing parameters unaltered. Another advantage of using ***nc***-PuO_2 compared to the conventional one, is the potential to reduce the sintering temperature and/or time to reach a similar microstructure, possibly coupling it with low-temperature oxidative sintering conditions [21]. On the other side, it remains to be evaluated whether the use of ***nc***-PuO_2 powder with high-surface area, might negatively impact the process depending on the aggregate's cohesion, because of possibly different dispersion and flowability behaviours. We did not perform in-detail studies in this regard, but the significantly higher bulk- and tap-densities of the mixtures made from ***nc***-PuO_2 compared to ***c***-PuO_2, suggest a better die-filling behaviour of the first.

The results suggest that the breaking up of the spheroid agglomerates of the ***nc***-PuO_2 in the initial milling stage is easier, leading to a better powder packing and distribution in the green pellets. The green density after pressing is slightly higher for ***nc***-PuO_2, and such trend is maintained after sintering.

The XRD data show a single-phase in the ***nc***-PuO_2 samples and incomplete solid-state interdiffusion using conventional powder. The reasons for the complete homogenisation can be *(i)* a better mixing during the milling phase, because of easier breaking of the softer agglomerates as mentioned above, and *(ii)* the smaller particle size of the PuO_2 primary particles. It is indeed well known, as well as intuitive, that homogenisation during sintering depends on such factors. An isothermal degree of homogenisation (H) has been defined as the point-to-point chemistry variation and expressed as [22,23]:

$$H \sim \frac{Dt}{\lambda^2}$$

where D is the diffusion coefficient of the controlling diffusion rate (which has the usual Arrhenius dependence on the temperature), t the time, and λ is the scale of the microstructural separation, or segregation length. The scale of separation depends among other, on particle size and initial mixing of the powder. A better mixing and smaller particle size will thus improve the homogenisation, as well as longer sintering times and higher temperatures.

Another effect that could explain the better homogenization of the two phases, is the enhanced diffusion-induced motion of grain boundaries at nanoscale. The solid solution formation during solid-state sintering is accompanied by the migration of the grain boundary at the interface between the two phases. The driving forces for this process are both of chemical nature (the reduction of the free energy due to formation of the solution, independent form grain size), and the pressure difference acting across a curved surface [24]. Such pressure is $\sim 2\gamma/r$, where γ is the grain boundary energy (typically in the order of 1.5 J/m^2 for UO_2 [25]), and r the grain boundary curvature radius, which is in the same order of the grain size (estimated at 18 nm for the ***nc***-PuO_2 powder), and can be estimated as ~80 MPa. For comparison, for a grain size of 200 nm, the driving force would be only ~8 MPa. Since the velocity of grain boundary migration is directly proportional to the driving force, it is clear how a nanocrystalline powder, if well-dispersed, yields faster homogenisation, which in turn favours faster densification and grain growth.

Conclusion

In the sintering of $(U,Pu)O_2$ mixed oxide pellets by milling and sintering of PuO_2 and UO_2 powders, the use of PuO_2 produced by an hydrothermal decomposition of oxalate process brings significant benefits compared to PuO_2 obtained from conventional thermal conversion of oxalates. Keeping all other processing parameters constant (*e.g.* UO_2 powder type and milling, pressing and sintering conditions), a single phase (XRD) with larger grain size is obtained when PuO_2 from hydrothermal decomposition is used. Such powder is composed of nanometric primary particles agglomerated in spherical granules. We interpret this result in terms of the shorter diffusion path for the solid solution formation, because of the smaller PuO_2 primary particle size and possibly an easier breaking of the agglomerates, and a higher driving force for grain boundary migration because of the highly curved interface between two phases. The implications for potential use in an industrial environment would have to be evaluated carefully, as nanocrystalline powders with high-surface area might show different dispersion and flowability features (a thorough powder characterization would be required). Moreover, other aspects such as repeatability and scalability of the results, as well as the effect of the introduction of scrap powder, are to be addressed.

CRediT authorship contribution statement

Jacobus Boshoven: Writing – review & editing, Methodology, Investigation. **Abibatou Ndiaye:** Writing – review & editing, Validation, Supervision, Project administration, Methodology, Conceptualization. **Bertrand Morel:** Writing – review & editing, Supervision, Project administration, Funding acquisition, Conceptualization. **Marco Cologna:** Writing – review & editing, Writing – original draft, Validation, Methodology, Investigation, Formal analysis, Data curation. **Jean-François Vigier:** Writing – review & editing, Methodology, Data curation. **Ramon Carlos Marquez:** Writing – review & editing, Investigation. **Rudy J.M. Konings:** Writing – review & editing, Writing – original draft, Validation, Supervision, Project administration, Formal analysis, Conceptualization. **Karin Popa:** Writing – review & editing, Writing – original draft, Validation, Supervision, Methodology, Investigation, Formal analysis, Data curation, Conceptualization.

Declaration of competing interest

The authors declare that they have no known competing financial interests or personal relationships that could have appeared to influence the work reported in this article.

Conflict of interest / Acknowledgements

The work was conducted under Third Party Work (TPW) contract 36376. We are grateful to JRC Analytical Services for chemical analysis and to Daniel Bouëxière, Herwin Hein and Octavian Vălu for technical support.

Data availability

Data will be made available on request.

References

[1] Y. Al-Douri, Metal Oxide Powder technologies. Fundamentals, Processing Methods and Applications, 1 ed., Elsevier, 2020, p. 446.
[2] D. Haas, MOX fuel fabrication experience at Belgonucleaire (IAEA-TECDOC–941), in: Recycling of plutonium and uranium in water reactor fuel. Proceedings of a technical committee meeting, 1997.
[3] M. Virot, T. Dumas, M. Cot-Auriol, P. Moisy, S. Nikitenko, Synthesis and multi-scale properties of PuO2 nanoparticles: recent advances and open questions, Nanoscale Adv 4 (2022) 4938–4971.
[4] O. Walter, K. Popa, O.Dieste Blanco, Hydrothermal decomposition of actinide(IV) oxalates: a new aqueous route towards reactive actinide oxide nanocrystals, Open Chem. 4 (1) (2016) 170–174.
[5] V. Petříček, M. Dušek, L. Palatinus, Crystallographic computing system JANA2006: general features, Z. Kristallogr. Cryst. Mater. 229 (5) (2014) 345–352.
[6] B. van Laar, H. Schenk, The development of powder profile refinement at the Reactor Centre Netherlands at Petten, Acta Cryst. A 74 (2) (2018) 88–92.
[7] G. Williamson, W. Hall, X-ray line broadening from filed aluminium and wolfram, Acta. Metall 1 (1) (1953) 22–31.

[8] M. Kato, A. Komeno, H. Uno, H. Sugata, N. Nakae, K. Konashi, M. Kashimura, Self-radiation damage in plutonium and uranium mixed dioxide, J. Nucl. Mater. 393 (1) (2009) 134–140.
[9] K. Popa, O. Walter, O.Dieste Blanco, A. Guiot, D. Bouëxière, J.-Y. Colle, L. Martel, M. Naji, D. Manara, A low-temperature synthesis method for AnO2 nanocrystals (An = Th, U, Np, and Pu) and associate solid solutions, CrystEngComm 20 (32) (2018) 4614–4622.
[10] D. Bouëxière, K. Popa, O. Walter, M. Cologna, Kinetic study on the grain growth of PuO2 nanocrystals, RSC Adv 9 (2019) 6542–6547.
[11] V. Baumann, K. Popa, O. Walter, M. Rivenet, G. Senentz, B. Morel, R. Konings, Synthesis of nanocrystalline PuO2 by hydrothermal and thermal decomposition of Pu(IV) oxalate: a comparative study, Nanomaterials 13 (2) (2023), pp. 320:1-10.
[12] G. Leinders, T. Cardinaels, K. Binnemans, M. Verwerft, Accurate lattice parameter measurements of stoichiometric uranium dioxide, J. Nucl. Mater. 459 (1–3) (2015) 135–142.
[13] R. Belin, P. Valenza, M. Reynaud, P. Raison, New hermetic sample holder for radioactive materials fitting to Siemens D5000 and Bruker D8 X-ray diffractometers: application to the Rietveld analysis of plutonium dioxide, J. Appl. Crystallogr. 37 (2004) 1034–1037.
[14] W. Su, L. Chen, W.S. Huo, W. Zhang, Y. Wang, Y. Zhou, Fracture mode transition from intergranular to transgranular in (TiZrNbTaCr)C: the grain boundary purification effect of Cr carbide, J. Eur. Ceram. Soc. 44 (4) (2024) 1881–1889.
[15] E. Holm, S. Foiles, How grain growth stops: a mechanism for grain-growth stagnation in pure materials, Science 328 (5982) (2010) 1138–1141.
[16] M.-M. Desagulier, J. Martinez, P. Martin, F. Lebreton, C. Guéneau, N. Clavier, Multi-scale structural investigation of uranium-plutonium mixed oxides (U1-yPuy) O2-x with high plutonium content, J. Nucl. Mater. 585 (2023), pp. 154645:1-11.
[17] F. La Lumia, L. Ramond, C. Pagnoux, P. Coste, F. Lebreton, J.-R. Sevilla, G. Bernard-Granger, Dense and homogeneous MOX fuel pellets manufactured using the freeze granulation route, J. Am. Ceram. Soc. 103 (5) (2020) 3020–3029.
[18] G. Kauric, O. Walter, A. Beck, B. Schacherl, O.Dieste Blanco, J.-F. Vigier, E. Zuleger, T. Vitova, K. Popa, Synthesis and characterization of nanocrystalline U1-xPuxO2(+y) mixed oxides, Mater. Today Adv. 8 (2020), pp. 100105:1-6.
[19] J.-Y. Colle, T. Wiss, O. Dieste, P. Pöml, D. Staicu, T. Tverberg, S. Bremier, R. Konings, V. Rondinella, T. Sonoda, A. Sasahara, S. Kitajima, Comparative study of fission product release of homogeneous and heterogeneous high-burn up MOX fuel by Knudsen Effusion Mass Spectrometry supported by EPMA, SEM/TEM and thermal diffusivity investigations, J. Nucl. Mater. 578 (2023), pp. 154340:1-18.
[20] D. Haas, J. Somers, F. Charollais, C. Fuchs, S. Foucaudot, Fabrication and characterization of MOX fuels with high plutonium content using alternative processes, in: International symposium on MOX fuel cycle technologies for medium and long term deployment, 17-21 May 1999, Vienna, 2020.
[21] J. Boshoven, J.-F. Vigier, P. Poeml, A. Ndiaye, B. Morel, R. Konings, K. Popa, M. Cologna, Low-temperature sintering of (U,Pu)O2 MOX in mild oxidative conditions, J. Nucl. Mater. 610 (2025), pp. 155800:1-7.
[22] M. Randall, J. Seong, Mathematical Relations in Particulate Materials processing: Ceramics, Powder metals, cermets, carbides, Hard materials, and Minerals, Wiley, 2008.
[23] M. Masteller, R. Heckel, R. Sekerka, A mathematical model study of the influence of degree of mixing and powder particle size variation on the homogenization kinetics of compacted blends of powders, Metall. Trans. A 6 (1975) 869–876.
[24] Y. Kaganovskii, L. Paritskaya, Size-dependent effects in low-temperature sintering and alloying of nanopowders, Powder Metall. Met. Ceram. 57 (2018) 421–430.
[25] E. Bourasseau, A. Mouret, P. Fantou, X. Iltis, R. Belin, Experimental and simulation study of grain boundaries in UO2, J. Nucl. Mater. 517 (2019) 286–295.